RESEARCH ARTICLE

Society For Biomaterials — WILEY

Decellularized peripheral nerve as an injectable delivery vehicle for neural applications

Deanna Bousalis[1] [ORCID] | Michaela W. McCrary[1] | Natalie Vaughn[1] | Nora Hlavac[1] | Ashley Evering[1] | Shruti Kolli[1] | Young Hye Song[1,2] | Cameron Morley[3] | Thomas E. Angelini[3] | Christine E. Schmidt[1]

[1]J. Crayton Pruitt Family Department of Biomedical Engineering, University of Florida, Gainesville, Florida, USA

[2]Department of Biomedical Engineering, University of Arkansas, Fayetteville, Arkansas, USA

[3]Department of Mechanical and Aerospace Engineering, University of Florida, Gainesville, Florida, USA

Correspondence
Christine E. Schmidt, J. Crayton Pruitt Family Department of Biomedical Engineering, University of Florida, Gainesville, P.O. Box 116131, FL 32611-6131, USA.
Email: schmidt@bme.ufl.edu

Funding information
National Heart, Lung, and Blood Institute, Grant/Award Number: 5F31HL150942-02; National Institute of Biomedical Imaging and Bioengineering, Grant/Award Number: 1R21NS111398-01

Abstract

Damage to the nervous system can result in loss of sensory and motor function, paralysis, or even death. To facilitate neural regeneration and functional recovery, researchers have employed biomaterials strategies to address both peripheral and central nervous system injuries. Injectable hydrogels that recapitulate native nerve extracellular matrix are especially promising for neural tissue engineering because they offer more flexibility for minimally invasive applications and provide a growth-permissive substrate for neural cell types. Here, we explore the development of injectable hydrogels derived from decellularized rat peripheral nerves (referred to as "injectable peripheral nerve [iPN] hydrogels"), which are processed using a newly developed sodium deoxycholate and DNase (SDD) decellularization method. We assess the gelation kinetics, mechanical properties, cell bioactivity, and drug release kinetics of the iPN hydrogels. The iPN hydrogels thermally gel when exposed to 37°C in under 20 min and have mechanical properties similar to neural tissue. The hydrogels demonstrate in vitro biocompatibility through support of Schwann cell viability and metabolic activity. Additionally, iPN hydrogels promote greater astrocyte spreading compared to collagen I hydrogels. Finally, the iPN is a promising delivery vehicle of drug-loaded microparticles for a combinatorial approach to neural injury therapies.

KEYWORDS
decellularization, hydrogel, injectable, neural injury, peripheral nerve, spinal cord injury

1 | INTRODUCTION

The nervous system is critical to almost all bodily functions, both voluntary and involuntary. Damage to the nervous system can cause severe impairment of sensory and motor function, paralysis, or even death. Although peripheral nerve has the inherent ability to regenerate over short distances, large defects require grafts for regeneration and functional recovery.[1] Further, the adult central nervous system

Deanna Bousalis and Michaela W. McCrary contributed equally to this study.

(CNS) has little inherent capacity to rehabilitate after injury,[1] and physical barriers such as glial scar formation after spinal cord injury (SCI) or traumatic brain injury (TBI) can further limit axonal regeneration.[2,3] Researchers have employed biomaterials strategies to address both peripheral and CNS injuries. For example, many peripheral nerve grafts and conduits have been developed from natural and synthetic polymers,[4] as well as decellularized peripheral nerve allografts.[5] Other researchers have explored filling such grafts with hydrogels, neurotrophic factors, aligned channels, and more[6-8] to facilitate axonal regeneration. Although multiple peripheral nerve grafts are on the

market, there are currently no FDA-approved therapies for CNS repair.[1,2,9] However, peripheral nerve grafts have proven beneficial for supporting regeneration in the CNS after injury.[10] Additionally, many pre-clinical studies and a few clinical trials have utilized biomaterial scaffolds for regeneration of the CNS after injury.[1,2,9,11]

A promising biomaterial strategy is the use of hydrogels for neural tissue engineering. Hydrogels are 3D hydrophilic polymer networks that swell within an aqueous environment and contain a high fraction of water but retain their mechanical structure through their cross-linked (chemical or physical) polymeric chains.[12-14] Hydrogels are typically soft and flexible materials that can easily match the mechanical properties of neural tissue.[15-19] This is important, as mechanical properties can drive cellular behavior, including neurite outgrowth.[16,18-20] The mechanical microenvironment also should closely match that of the target tissue as to not cause additional injury or inflammatory responses.[21-26] Structurally, hydrogels contain pores, which, if sized appropriately, facilitate cellular growth/infiltration as well as nutrient and waste exchange.[15,17,19] Another advantage of hydrogels is their amenability to be incorporated with other approaches to generate combinatorial therapies.[15,17] When used with cell transplantation strategies, hydrogels provide a growth substrate that can promote transplanted cell survival and integration into host tissue.[18,19] When combined with pharmaceutical strategies, hydrogels can be used as a depot or sustained drug delivery vehicle for these interventions.[15,18,19]

One of the most notable practical advantages of hydrogels for CNS repair is that they can be injectable.[15,17-19,27] Most clinical cases of SCI are contusion injuries, resulting in lesions with highly irregular geometries that form over time.[27] Lesion spaces can also form in the brain after traumatic insult or ischemic stroke.[9] Injectable biomaterials can better and more consistently conform to these irregular lesion spaces compared to traditional pre-formed scaffolds.[15,18,19] Injectability further allows for a minimally invasive therapeutic strategy that can reduce additional tissue damage and surgical complications.[17-19,27] Additionally, injectable hydrogels can be used as fillers in peripheral nerve guidance conduits to promote a more robust growth response and provide a supportive microenvironment.[28,29]

Numerous preclinical studies have been performed with hydrogel materials such as agarose,[30,31] hyaluronic acid,[32,33] methylcellulose,[34] fibrin,[31,35] alginate,[36,37] collagen,[38-40] silk,[41] Matrigel,[38] and self-assembling peptides.[42,43] Although many of these hydrogel strategies have shown therapeutic promise, few of them accurately recapitulate the native extracellular matrix (ECM) composition of the nervous system. In this manner, a hydrogel derived from decellularized neural tissue could be advantageous over the majority of other hydrogel or polymer scaffold options explored thus far. A unique attribute of decellularized tissues (commonly referred to as decellularized ECM or "dECM") is their ability, upon appropriate conditions, to be processed into a homogenous precursor solution that forms a hydrogel upon injection into the injury site in vivo or incubation at 37°C.[44] This results in a less invasive procedure compared to those involving scaffold implantation.[45] Although dECM hydrogel scaffolds have been used as treatments themselves, they have also successfully been combined with other therapies to serve as delivery vehicles for cells, drugs, or other bioactive molecules.[44,45] For example, decellularized canine sciatic nerve has been used as a hydrogel filler for nerve conduits after peripheral nerve injury.[28] In addition, decellularized brain-derived hydrogels have been explored as a treatment after SCI in rats.[46]

Previously, our group developed injectable hydrogels derived from decellularized rat peripheral nerve (referred to as "injectable peripheral nerve [iPN] hydrogels"), based on the Hudson decellularization method.[47] Cornelison et al. has demonstrated that iPN hydrogels improve functional outcome after SCI.[48] Additionally, Cerquiera et al. has demonstrated the potential of the iPN hydrogel to serve as a carrier for Schwann cells as an injectable SCI therapy.[49] Unfortunately, despite these promising results, the primary chemical detergent used in the Hudson decellularization method, Triton X-200, was discontinued by the manufacturer in recent years. McCrary et al. reoptimized the rat peripheral nerve chemical decellularization process[50] with chemical detergent sodium deoxycholate to be comparable to or better than the previously used Hudson method[47] with respect to intracellular protein removal and ECM preservation. More specifically, McCrary et al. found that replacing Triton X-200 with 3% sodium deoxycholate and an incubation in deoxyribonuclease (DNase) resulted in equivalent decellularization profiles, as well as comparable cytocompatibility. This new method has been titled the "SDD method".[50]

Here, we explore the development of injectable hydrogels derived from rat peripheral nerves decellularized using the newly developed SDD method, and compare to hydrogels composed of collagen I, the primary ECM component in peripheral nerve and a common biomaterial used for a variety of tissue engineering applications,[51] including neural regeneration.[52,53] To our knowledge, this is the first study to utilize the novel SDD method decellularization protocol to develop injectable hydrogels. Here we assess the gelation kinetics, mechanical properties, cell bioactivity, and drug release kinetics of the updated iPN hydrogel to characterize and showcase its potential as an injectable delivery vehicle for neural applications.

2 | MATERIALS AND METHODS

2.1 | Nerve harvest and decellularization

All animal work in this study was approved by the Institutional Animal Care and Use Committee (IACUC) at the University of Florida. Adult male and female Sprague Dawley rats (250–300 g) were obtained from Charles River (Wilmington, MA) and cared for by Animal Care Services in accordance with IACUC standards and the Animal Welfare Act. Rats had access to 12-h light/dark cycles and standard water and food. Prior to nerve harvest, rats were euthanized using American Veterinary Medical Association Guidelines using carbon dioxide. Sciatic nerves (about 3 cm in length) were harvested aseptically, and epineurium were removed from the nerves using sterile forceps. Nerves were then transferred to fresh 1X phosphate buffered saline (PBS) and frozen at −20°C until decellularization.

The decellularization protocol of sciatic nerves was previously published.[50] Briefly, nerves were subjected to washes in water, salt

buffers, zwitterionic detergents sulfobetaine-10 (SB-10, Sigma-Aldrich D4266) and sulfobetaine-16 (SB-16, Sigma-Aldrich H6883), anionic detergent sodium deoxycholate (SD, Sigma-Aldrich D6750), and enzymes chondroitinase ABC (ChABC, Sigma-Aldrich C3667) and deoxyribonuclease I (DNase, Sigma-Aldrich D4527). All steps except enzyme (DNase and ChABC) incubations were conducted under orbital agitation. All washes and incubations were performed at room temperature[50] except for ChABC, which was incubated at 37°C. To demonstrate decellularization, unprocessed and decellularized rat sciatic nerve sections were immunostained as described previously.[50]

2.2 | iPN hydrogel fabrication

Decellularized peripheral nerves were solubilized using a method adapted from Cornelison et al.[48] Immediately after the decellularization process, processed nerves were subject to three 15-min washes in sterile ddH$_2$O on an orbital rotator, flash-frozen in liquid nitrogen, and then lyophilized (Labconco) for 3 days. Lyophilized nerves were weighed and minced into approximately 1-mm pieces in a scintillation vial (Millipore Sigma). 1 mg/ml pepsin (Sigma Aldrich P7012) in 0.01 M hydrochloric acid (Sigma Aldrich 258,148) was added to achieve tissue concentrations of 5–20 mg of tissue per 1 ml of pepsin solution. Vials were capped, sealed with parafilm (Bemis Company, Inc.), and incubated for 72 h at room temperature under constant agitation through use of a magnetic stir bar (SEOH 001.1206CS). Nerve digests, which at this point were homogenous solutions, were transferred from scintillation vials into microcentrifuge tubes and placed on ice. 1 M NaOH (Sigma-Aldrich 221,465) was added to the digests until the pH reached 7.4 to neutralize the solution, and the solution was stabilized by adding 10X PBS at an amount 1/9th the volume of digest. This resulting solution will henceforth be referred to as "pre-gel solution." In the subsequent text, hydrogels will be referred to in terms of initial decellularized tissue concentration prior to digest and neutralization (e.g., 7.5 and 10 mg/ml iPN hydrogels contained 7.5 and 10 mg decellularized lyophilized nerve per ml of pepsin solution, respectively, which becomes 6.75 and 9 mg/ml after neutralization and stabilization, respectively).

Hydrogels were first assessed qualitatively for ability to form hydrogels (n = 3 separate digests consisting of at least two separate peripheral nerves). 30 μl of pre-gel solution was pipetted onto parafilm-coated plastic dishes and incubated at 37°C (humidified) for up to 1 h. Gelation was then assessed based on handling of the hydrogel (ability to scoop it up with a spatula while it maintains shape) and submersion in 1X PBS (whether the hydrogel remained intact or quickly dissolved).

When using iPN for cell culture experiments, the digest was performed under aseptic conditions. Sterility was maintained throughout the decellularization process and lyophilization as described in previous sections. To ensure sterility during hydrogel fabrication, all spatulas, instruments, vials, and so forth, were autoclaved. All solutions were either autoclaved or filter sterilized prior to being used. Magnetic stir bars were soaked in 70% ethanol for at least 30 min before being placed into the vial with nerve tissue pieces. All parts of the

digestion process, including measuring/weighing reagents, mincing tissue, neutralizing, and so forth, were performed in a biological safety cabinet (BSC).

2.3 | Collagen hydrogel fabrication

For all assessments, except qualitative gelation, rat-tail collagen I hydrogels (Corning 354249) served as controls. Collagen I hydrogels were prepared at concentrations analogous to iPN hydrogel final concentrations (6.75 and 9 mg ECM per ml solution after neutralization and stabilization) based on the stock collagen I concentration provided by the manufacturer. Collagen I hydrogels were prepared by mixing rat-tail collagen I with a DMEM/HEPES solution consisting of 23.25 mg/ml of sodium bicarbonate (JT Baker 3509–01) in 10X DMEM (Sigma-Aldrich D2429) and HEPES buffer (Fisher SH3085101) mixed 1:1 to form 5× DMEM/HEPES. Final collagen pre-gel solutions always contained 20% DMEM/HEPES solution and 80% collagen I solution. The collagen I was diluted to the appropriate concentration with 0.02% acetic acid (Fisher BP2401), as this was the solvent the collagen was received in from the manufacturer. When using collagen I hydrogels for cell culture experiments, all parts of the fabrication process were performed inside a BSC with sterile materials.

2.4 | Turbidity gelation kinetics assessment

Turbidity gelation kinetics (n = 3 separate digests consisting of at least two separate peripheral nerves) was conducted as previously described by Medberry et al.[54] to determine gelation parameters. Briefly, a SpectraMax® M5 microplate reader (Molecular Devices) was heated to 37°C. Separately, 150 μl of decellularized nerve pre-gel solution or collagen I was added to a 96-well plate. To minimize any potential evaporation during turbidity measurements, approximately 200 μl of 1× PBS was added to multiple wells around the perimeter of the plate. This plate was then immediately transferred to the pre-heated plate reader. The absorbance of the samples at 405 nm was read every 30 s for up to 60 min. Absorbance data were then normalized according to Equation (1).[54]

$$\text{Normalized Absorbance}\,(NA) = \frac{A - A_0}{A_{max} - A_0} \qquad (1)$$

In Equation (1), A represents the instantaneous absorbance of the solution at a given time, A_0 represents the initial absorbance (at time = 0), and A_{max} represents the maximum absorbance measured in the experiment. Normalized values were then plotted against time to depict gelation as it occurs over time (based on opacity). Time to reach 50% of gelation (t_{50}) (when NA = 0.5), time to reach 95% of gelation (t_{95}) (when NA = 0.95), speed of gelation (slope of linear region of the curve), and time until gelation is initiated (t_{lag}) (time until the linear region begins) were determined graphically. These values were then compared between the different tissue concentrations and hydrogel type.

2.5 | Confocal reflectance imaging

Confocal reflectance imaging was used to validate collagen-based gelation kinetics and to visualize the collagen structure within the hydrogel. iPN and collagen hydrogels ($n = 3$ hydrogels per concentration and material type, 50 μl total volume each) were cast in glass-bottomed plastic dishes (Cellvis). Hydrogel collagen fibrillar structure was imaged at 60X magnification (oil immersion objective) and 488 nm light via confocal laser scanning microscopy equipped with a reflectance filter cube (Nikon Eclipse Ti-E, Nikon Instruments). Representative Z-stack images (5 μm) from each sample type were collected, and a maximum intensity projection image was generated using NIS-Elements software (Nikon Instruments).

2.6 | Mechanical characterization

To determine compressive mechanical properties, meso-scale indentation was utilized ($n \geq 6$ per concentration and material type). To do so, iPN and collagen pre-gel solutions were cast in 5-mm diameter, 1.5-mm height silicone molds and allowed to gel at 37°C for at least 30 min. The molds were then removed, and the hydrogels were submerged in 1X PBS within a small plastic dish. Indentation was conducted using a Hysitron indenter equipped with a 3-mm spherical probe (Bruker Nano Surfaces Nanomechanical Test Instruments). All samples were indented to a depth of 150 μm (∼10% sample height) at 20 μm/s with a 3-mm spherical probe.[55] The maximum depth was then held for 60 s before retraction. This process was repeated at least three times per individual hydrogels in the same location, with approximately 2 min between each reading. An analysis method described in Stewart et al.[56] was utilized. Briefly, MATLAB was used to convert force readings from the indenter into effective modulus values using the Hertz contact model equation.[57,58] These modulus values relative to time were fit to the Standard Linear Solid model for viscoelastic materials[59] to obtain useful metrics such as steady state modulus (SSM) and characteristic time. Data were not used if the resulting normalized mean squared error was < 0.4, thus indicating a poor fit.[56]

Rheological properties (storage and loss moduli) of iPN and collagen I hydrogels were determined using rheology (rheometer from Anton Paar, Austria) ($n \geq 5$ per concentration and material type). For this assessment, iPN and collagen I pre-gel solutions were added to 8.5 mm diameter, 1.5 mm height silicone molds and incubated at 37°C for 30 min. Hydrogels were then removed from the molds and allowed to equilibrate in 1X PBS at room temperature overnight. Hydrogel samples were placed on the bottom plate of the rheometer. Water was added to humidity chamber to ensure hydrogels would not dry out during measurement. The top plate of the rheometer (8 mm sandblasted parallel plate [PP08] from Anton Paar, Austria) was then lowered until flush with the hydrogel surface. An amplitude sweep was conducted with a range of 0.01% to 100% strain (angular frequency of 6.3 rad/s) to determine the linear viscoelastic region. A strain of 0.5% (within linear viscoelastic region) was selected as the amplitude for the frequency sweep. The viscoelastic properties were then measured at 0.5% strain at angular frequencies ranging from 0.1 to 100 rad/s. Storage and loss modulus within this frequency range was calculated and reported by Rheoplus Software (Anton Paar, Austria) which is the computer interface for the rheometer.

2.7 | Swelling studies

Fully formed iPN and collagen I hydrogels ($n = 3$ per concentration and material type, 50 μl total volume) were incubated in excess 1X PBS for 24 h at room temperature. Hydrogels were rinsed with water and wet weights measured. The three hydrogels for each were then pooled (total of 150 μl volume), frozen at −80°C, and lyophilized (Labconco). Samples were pooled due to the weights of individual hydrogels being less than the mass balance limit of detection. After lyophilization, the dry weight of the pooled samples was recorded. The swelling ratio was then determined using Equation (2). In Equation (2), W_s is the sum of the swollen masses and W_d is the pooled dry weight.

$$\text{Swelling ratio (SR)} = \frac{W_s - W_d}{W_d} \qquad (2)$$

24 h was selected as the duration for the swelling experiment because, in literature, collagen-based hydrogels have been found to reach swelling equilibrium in 24 h or less.[60-62] Additionally, 24 h for the swelling duration is fairly standard for collagen-based hydrogels.[63-67]

2.8 | Degradation studies

Fully formed iPN and collagen I hydrogels ($n = 3$ per concentration and material type, 50 μl volume) were incubated in a 24-well plate containing 300 μl 1X PBS at 37°C under gentle agitation (30 RPM shaking). Wet weights were measured every day for 30 days. Percent weight loss was calculated using Equation (3). In Equation (3), W_t represents instantaneous wet weight at time t and W_0 denotes the initial wet weight.

$$\text{Percent weight loss (\%WL)} = \left(\frac{W_t - W_0}{W_0} \right) \times 100 \qquad (3)$$

2.9 | Schwann cell culture and seeding

Primary rat Schwann cells were purchased from ScienCell (R1700). Tissue culture-treated flasks were first coated with laminin (Trevigen 3446–005-01) by incubating with 2 μg/ml laminin solution for 30 min in a 37°C incubator, then rinsing once with sterile ddH$_2$O. Schwann cells were then thawed or passaged into the flasks and grown in medium composed of DMEM (Fisher Scientific MT10013CV) with 10% fetal bovine serum (FBS, Atlanta Biologicals S11150), 1%

penicillin/streptomycin (Thermo Fisher Scientific 15-140-122), 0.1% forskolin (Sigma-Aldrich F3917), 0.135% bovine pituitary extract (Gibco 13028014), and 0.1% basic fibroblast growth factor (Gibco PHG0264). A half media change was performed the day after thawing and a full media change was performed every 3 days thereafter.

For seeding Schwann cells into hydrogels, P3-P6 Schwann cells were rinsed with sterile 1X PBS, incubated in 0.25% Trypsin–EDTA (Thermo Fisher 25200072) for about 3 min until cells were no longer adherent to the bottom of the flask, and neutralized with an equal amount of growth medium. Cells were then transferred to a conical tube and pelleted by centrifugation. Supernatant was aspirated and cells were resuspended in 1–3 ml of Schwann cell growth medium, then counted on a Countess automated cell counter (Invitrogen). Cells were pelleted again and resuspended at a concentration of 8.33 million cells/ml. Cell suspension was next added in an amount 1/10th that of the final volume of pre-gel solution. For example, 10 μl cell suspension was added to 90 μl of pre-gel solution to make a final total of 100 μl pre-gel solution containing cells at a final concentration of 8.33×10^5 cells/ml. Pre-gel solutions containing cells were then pipetted into silicon molds and incubated for at least 30 min at 37°C. Each hydrogel was 30 μl volume and contained 2.5×10^4 cells. Hydrogels were transferred to a 24-well plate with a sterile spatula and 450 μl growth medium was added to each well. Hydrogels were cultured for 3 days, after which Live/Dead staining and/or an alamarBlue metabolic assay was performed.

2.10 | Astrocyte co-culture and seeding

Brain cortices were isolated from post-natal day 2–3 Sprague Dawley rat pups, enzymatically digested, and cultured as described by Hlavac et al.[68] Seven days after isolation, cultures were mechanically agitated to purify astrocytes from other glia, namely microglia. The remaining "astrocyte co-cultures" contain a majority astrocytes (> 70% GFAP-positive in culture) with some other adherent cells, like fibroblasts and endothelial cells as part of the isolation technique.[69] Astrocytes were grown in medium consisting of DMEM-F12 (Caisson Labs DFL15), 10% FBS, and 1% P/S with full media changes every 3 days until confluent. Astrocytes were encapsulated in hydrogels at 5×10^5 cells/ml final concentration, or 1.5×10^4 cells per 30 μl hydrogel, using the method as described above for Schwann cell encapsulation. Astrocytes were cultured for 3 days, after which cells and hydrogels were fixed and stained for glial fibrillary acidic protein (GFAP) as described below.

2.11 | Determination of cell viability and metabolic activity

Live/Dead Cytotoxicity staining (Life Technologies L−3224), consisting of calcein AM and ethidium homodimer-1, was performed on Schwann cells cultured in hydrogels. Cells were incubated in a working solution of 2 μM calcein AM and 4 μM ethidium homodimer-1 in 1× DPBS for 30–45 min at 37°C. Working solution was then

aspirated, and 1X DPBS was added to cells. DPBS was removed from each well immediately before imaging on a Zeiss LSM 880 confocal microscope.

An alamarBlue metabolic assay was performed on Schwann cells cultured in hydrogels. Media was aspirated from cells, and 450 μl of an alamarBlue working solution consisting of 10% alamarBlue reagent (Thermo Scientific DAL1100) in Schwann cell growth medium was added to each well. Cells were incubated in working solution for 2 h at 37°C to allow cells to metabolize and reduce the resazurin in the alamarBlue reagent into resofurin. Working solution was then pipetted into a black, clear-bottom 96-well microplate and read on a Molecular Devices m5e microplate reader at an excitation wavelength of 545 nm and emission of 590 nm. All alamarBlue absorbance values were normalized to the collagen I absorbance values for individual experimental runs.

2.12 | Hydrogel processing and immunostaining

Astrocytes were cultured in hydrogels for 3 days then fixed by incubating in 2% paraformaldehyde (PFA, Fisher Scientific AAJ19943K2) for 30 min at room temperature. PFA was then washed out with three 15-min PBS soaks. Hydrogels were next transferred to microcentrifuge tubes using spatulas and soaked in 30% sucrose with 1 mg/ml sodium azide in PBS solution overnight at 4°C to prevent ice crystal formation when freezing. The following day, hydrogels were placed in plastic cryomolds and covered with optimal cutting temperature compound (Electron Microscopy Sciences 62,550). Molds were placed in a humidified sealed box and placed at 4°C overnight. Then, molds were flash-frozen by briefly dipping in liquid nitrogen and quickly moving to −20°C, where they were stored in sealed plastic bags until sectioning. Hydrogels were next cut into 15-μm thin cryosections using a Leica cryostat. Sections were either heated for 2 h on a slide warmer or left overnight at room temperature and stored at −80°C until immunostaining was performed.

For immunostaining, slides were warmed for at least 30 min on a slide warmer and soaked in PBS twice for 5 min each, then water for 5 min to remove residual OCT. A hydrophobic barrier was drawn around the sections on the slide using a PAP Pen (Electron Microscopy Sciences 71312). Samples were permeabilized in 0.5% Triton X-100 (Sigma-Aldrich 93443) in PBS for 15 min, washed with PBS for 10 min, and blocked for 1 h in 5% bovine serum albumin (BSA, Sigma-Aldrich A9418). After blocking, samples were incubated in primary antibody GFAP solution at a dilution of 1:350 in 5% BSA overnight at 4°C. Primary antibodies were next removed using three 10-min washes with PBS-T (PBS with 0.1% Tween-20), and sections were incubated in secondary antibody solution for 1 h at room temperature. Secondary antibody used was Alexa Fluor 568 Goat anti-rabbit IgG (H + L) (Invitrogen A11011) at a 1:1000 dilution in 5% BSA. Secondary antibodies were removed with three 10-min PBS-T washes, and then sections were incubated in DAPI solution (1:1000 in ddH$_2$O), followed by one 10-min PBS wash. Coverslips were subsequently mounted onto slides with Fluoromount G mounting medium (Fisher

Scientific OB100-01) and left to dry overnight at room temperature. The next day, coverslips were lined with clear nail polish to preserve the samples. Slides were imaged on either a Zeiss Axio Imager Z2 microscope or a Zeiss laser scanning confocal microscope 880.

2.13 | Image analysis

To determine astrocyte spreading, the average area covered by each astrocyte per hydrogel section was calculated. The image of the channel of interest was opened in ImageJ and converted to 32-bit grayscale images. Images were then thresholded to highlight the cells stained and to eliminate background noise. The scale was set for each individual image. Either the circle tool or the freehand selection tool was used to select the hydrogel section in the image. Then, an area measurement was taken. If there were shape irregularities in the images (e.g., rip in the hydrogel section), multiple smaller selections were made and measured instead, and then averaged together per sample for analysis. The total area covered by astrocytes was divided by the number of astrocytes in each image (also counted in ImageJ) to obtain the "Average Astrocyte Area" metric. To determine average circularity of astrocytes, images were converted to 32-bit, thresholded as described above, and the "analyze particle" function was used to obtain measurements of shape descriptors for each cell.

2.14 | PLGA microparticle synthesis

50/50 DL-Lactide/glycolide copolymer (Purasorb PDLG, Corbion 5004A), which will be referred to as PLGA, was thawed in a desiccator for 15 min to come to room temperature and weighed. Five percent (wt/vol) PLGA was dissolved in dichloromethane (Sigma-Aldrich, 270997) in a glass vial. The vial was placed on a shaker plate at 150–200 rpm for approximately 10 min until the PLGA was dissolved completely. 20 kDa fluorescein isothiocyanate-dextran (FITC-dextran, Sigma-Aldrich FD20) was dissolved at 5 mg/ml in ddH$_2$O. 1 ml of the FITC solution was added to the PLGA/DCM solution. For blank particles, 1 ml of ddH$_2$O was added. The solution was vortexed for 2 min and sonicated with no heat to allow the FITC-dextran to dissolve completely. The solution was homogenized for a total of 2 min using a tissue master homogenizer (Omni TM125-115). The speed was increased every 15 s for a minute until the homogenizer was on maximum speed, then the solution was homogenized for another minute at maximum speed to form the primary emulsion. The entire primary emulsion was added to 50 ml of 5% (wt/vol) polyvinyl alcohol (PVA, MP Biomedicals 151937) solution in ddH$_2$O, and homogenized for another 2 min as described to form the secondary emulsion. The entire secondary emulsion was added to 500 ml of 1% (wt/vol) PVA solution in an Erlenmeyer flask. A magnetic stir bar was added, and the flask was placed on a stir plate set to 300 rpm. The mouth of the Erlenmeyer flask was covered with parafilm and small holes were made with forceps. The solution was left spinning in the chemical fume hood overnight to allow residual DCM to evaporate. For emulsions containing FITC-dextran, the flasks were covered with aluminum foil to protect them from light.

The next day, the solution from the flasks was collected in 50 ml conical tubes and centrifuged at 400 G for 10 min to collect microparticles. The supernatant was discarded and 35 ml of ddH$_2$O was added to wash the particles. Particles were centrifuged again, and the wash step was repeated three more times. After the final wash step, excess water was removed from tubes, and particles were flash frozen in liquid nitrogen. Tubes were quickly covered with parafilm, small holes were poked through with forceps, and particles were lyophilized for at least 72 h on a Labconco lyophilizer. After removal from the lyophilizer, particles were stored at −20°C until use.

Particle size and loading efficiency was characterized as described in the Supplemental Information S1. Mean particle diameter was 2.33 μm and loading efficiency was 16.04%.

2.15 | FITC-dextran in vitro release studies

Decellularized rat peripheral nerves were digested to create iPN hydrogel pre-gel solutions as described previously. For initial study with free FITC-dextran in iPN, solubilized FITC-dextran (in water) was added to iPN such that the final concentration of pseudo-drug was 1 mg/ml. Hydrogels (50 μl volume) were then formed through incubation at 37°C and placed into a 48-well plate containing 250 μl of 1X PBS. For PLGA studies, FITC-dextran-loaded microparticles were weighed and mixed with iPN pre-gel solution at the concentration of 750 μg particles per 30 μl of pre-gel solution. Solutions were mixed using a pipette tip to ensure particles were homogeneously dispersed, and then a chilled pipette tip was used to transfer the particle/pre-gel solution into 30-μl silicone molds. Molds were then incubated at 37°C for 30 min to initiate gelation. Hydrogels were removed from the molds and placed in 24-well plates in 750 μl of 1X PBS. Experimental control groups included blank particles and FITC-dextran particles dissolved at the same concentration as those inside the gel (750 μg particles per 750 ml of PBS). For both studies, plates were placed on a shaker plate at 37°C gently shaking at 50 rpm. At each experimental time point (1, 6, 24, 48, and 72 h) eluates were collected. All the PBS from the hydrogel wells were collected in individual microcentrifuge tubes, and fresh PBS was added to the wells. For the free particle groups, all PBS volume was collected in individual microcentrifuge tubes and centrifuged at 400 G for 10 min to spin down the remaining particles. The supernatants were collected, and the remaining particles were resuspended in fresh PBS and added back to the well plate.

To determine the concentration of FITC in the eluates, FITC-dextran was dissolved in PBS at 1 mg/ml. A serial dilution was then performed on this solution to create a standard curve of FITC-dextran concentration when reading the fluorescence on a plate reader. A volume of 150 μl of each standard was added to a clear-bottomed black 96-well plate in duplicate. A volume of 150 μl of each eluate sample was also added to the well plate. Plates were read on a Molecular Devices m5e microplate reader with an excitation of 490 nm and emission of 520 nm. The fluorescence values of the standards were

then graphed against their known concentrations to create a standard curve. A trendline was fit to the standard curve to obtain an equation from which the concentration of each elution sample can be calculated based on its fluorescence value.
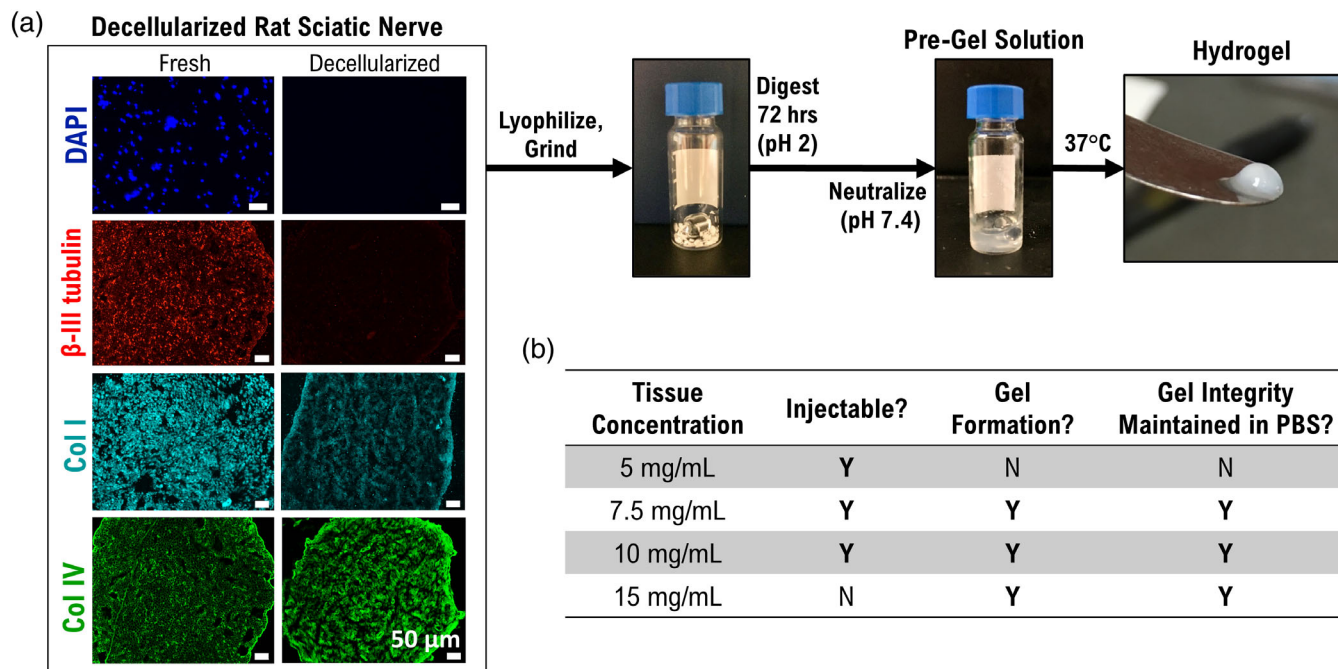
2.16 | Statistics

For all experiments, unless otherwise noted, at least three separate decellularized nerves (separate donors) or digests (generated from separate donors) were analyzed. Additionally, owing to potential variability between decellularization batches, care was taken to use samples from the same batch of decellularized nerves for any individual study. Statistical analyses were performed in GraphPad Prism 6, which included ordinary one-way ANOVA tests followed by Tukey's post-hoc multiple comparisons test for comparisons of more than two groups. Brown–Forsythe tests were used to test for equal variance among groups. When unequal variances and non-normality were detected, a Kruskal–Wallace test was performed followed by Dunn's multiple comparisons test. For comparisons between only two groups, two-tailed t-tests were performed with F tests to compare variances. When variances were not equal between two groups, a Mann–Whitney test was performed. Outliers were eliminated using Grubbs test. All graphing was also performed in GraphPad Prism 6. All data are presented as mean ± SD unless otherwise noted. Significance was defined as $p < 0.05$.

3 | RESULTS

3.1 | Fabrication of decellularized peripheral nerve-derived hydrogel

After decellularization of rat sciatic nerves, immunostaining was performed to demonstrate (a) appropriate removal of nuclei (DAPI) and intracellular protein β-III tubulin and (b) preservation of ECM proteins collagen I and collagen IV (Figure 1(A)).

To optimize hydrogel fabrication, decellularized nerves were solubilized at concentrations ranging from 5 to 20 mg decellularized tissue per milliliter of pepsin/acid solution. Methodology is pictured in Figure 1(A). These hydrogels were then qualitatively assessed for gelation by gently handling and submersing in 1X PBS to observe dissolution. Figure 1(B) summarizes the results of the qualitative assessments. At the highest concentration (20 mg/ml), the tissue failed to fully digest into a homogenous pre-gel solution; there was evidence of pieces of intact nerve. Therefore, these samples were not assessed for gelation. When the concentration was decreased to 15 mg/ml, digestion was deemed successful, as the pre-gel solution was homogenous and free from residual pieces of tissue. Although these samples produced hydrogels that maintained their shape and could be handled, this concentration was extremely viscous, and injection was not practical. Lower concentrations of 10 and 7.5 mg/ml were easily injected and resulted in stable hydrogels. Hydrogels from

Tissue Concentration	Injectable?	Gel Formation?	Gel Integrity Maintained in PBS?
5 mg/mL	Y	N	N
7.5 mg/mL	Y	Y	Y
10 mg/mL	Y	Y	Y
15 mg/mL	N	Y	Y

FIGURE 1 Overview of hydrogel fabrication process. (A) Rat sciatic nerve was decellularized, as indicated through removal of cell nuclei (DAPI, blue) and neurons (β-III tubulin, red), as well as preservation of extracellular matrix proteins collagen I (light blue) and collagen IV (green) (Images are representative samples from a set of at least $n = 3$ distinct nerves). Decellularized nerve was lyophilized and ground into small pieces which were then digested in acidic solution for 3 days. After neutralization, a homogenous and injectable "pre-gel solution" exists which forms a hydrogel upon exposure to body temperature, or 37°C. (B) Table of nerve tissue concentrations tested for ability to form a hydrogel. Solutions were qualitatively assessed for injectability, gel formation upon heating, and whether the hydrogel maintained integrity after submersion in 1X PBS
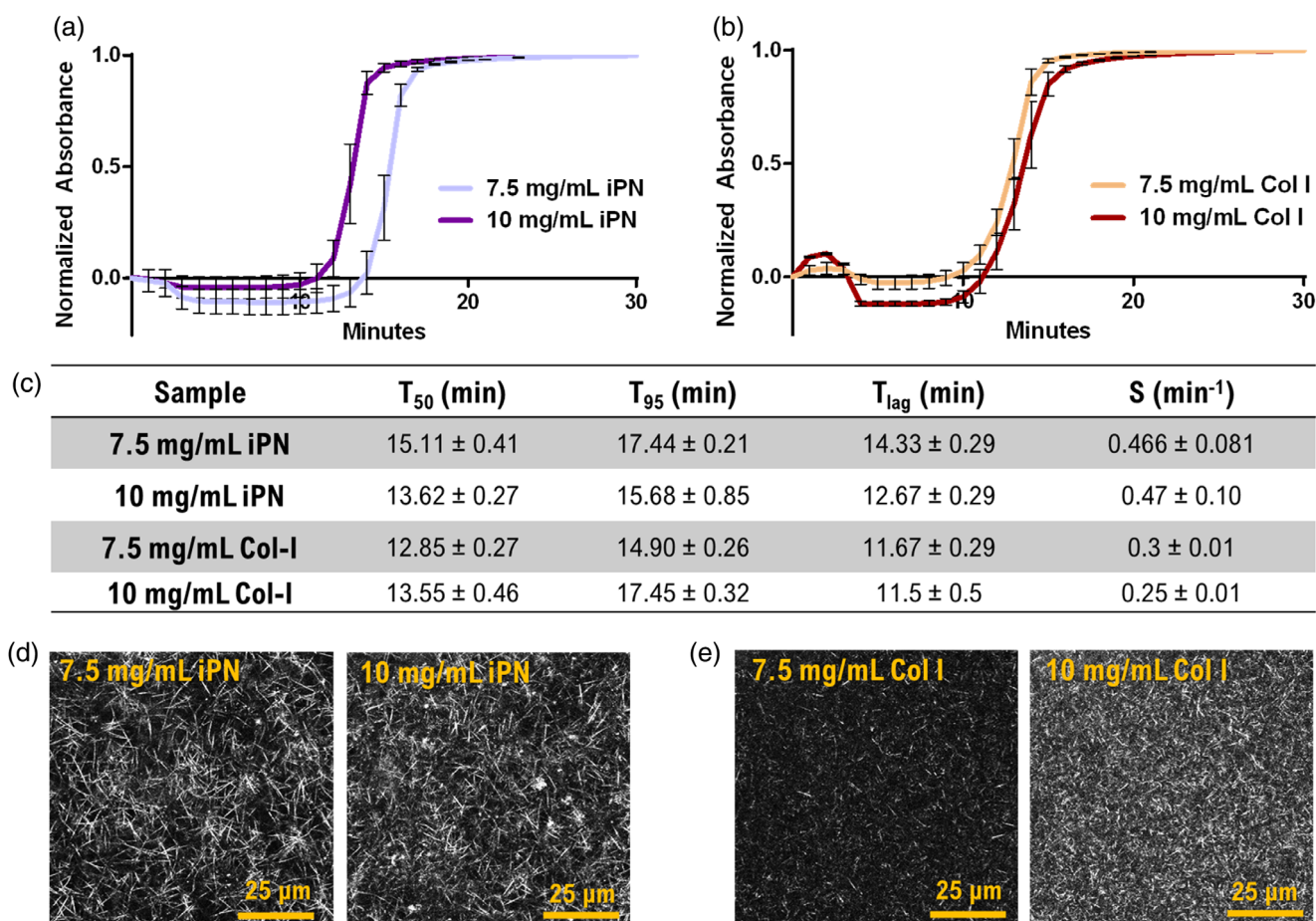
both concentrations could be handled and submerged in 1X PBS without losing their shape. Finally, at the 5 mg/ml concentration, no hydrogel formation was observed.

3.2 | Gelation properties of iPN hydrogel

To understand characteristics of the gelation process, turbidity gelation kinetics were assessed. The turbidity gelation kinetic profiles for iPN and collagen I hydrogels are summarized in Figure 2. Collagen I was used as a control because this material is widely used in literature for a variety of tissue engineering applications,[51] including neural regeneration,[52,53] and its properties are well studied.[70] Additionally, this ECM component is abundant in peripheral nerve tissue,[53] plays an important role in CNS development,[71] and is hypothesized to be the main component giving rise to the thermal gelling properties of iPN.[48] Overall, the iPN hydrogels had similar sigmoidal gelation curves as collagen I, which is indicative of collagen fibrillogenesis.[72] Briefly, it is believed that collagen fibril formation, or collagen fibrillogenesis,

occurs as a result of hydrophobic interaction between collagen molecules and their tendency to minimize the number of hydrophobic residues exposed to water by burying them within the fibril.[73,74] This loss of water from bound collagen monomers is associated with increased entropy.[44] Further comparison of gelation kinetic parameters is summarized in Figure 2(C). Lag time until gelation initialization differed between groups and concentrations. For the iPN hydrogels, the 7.5 mg/ml hydrogels had a significantly longer lag time (14.33 ± 0.29 min) compared to 10 mg/ml iPN (12.67 ± 0.29 min) ($p < 0.05$). For the collagen I hydrogels, no significant difference in lag time was detected between 7.5 and 10 mg/ml (11.67 ± 0.29 min and 11.50 ± 0.50 min, respectively). Upon comparison of the 7.5 mg/ml iPN and collagen I samples, the iPN was found to have a significantly longer lag time compared to its collagen counterpart ($p < 0.05$).

The time to reach 50% gelation (t_{50}) also varied based on material and concentration. For the iPN hydrogels, the 7.5 mg/ml concentration t_{50} was significantly slower than the 10 mg/ml iPN (15.11 ± 0.41 min and 13.62 ± 0.27 min, respectively) ($p < 0.05$). Interestingly, this trend was not observed in collagen I hydrogels, as t_{50} was

Sample	T_{50} (min)	T_{95} (min)	T_{lag} (min)	S (min^{-1})
7.5 mg/mL iPN	15.11 ± 0.41	17.44 ± 0.21	14.33 ± 0.29	0.466 ± 0.081
10 mg/mL iPN	13.62 ± 0.27	15.68 ± 0.85	12.67 ± 0.29	0.47 ± 0.10
7.5 mg/mL Col-I	12.85 ± 0.27	14.90 ± 0.26	11.67 ± 0.29	0.3 ± 0.01
10 mg/mL Col-I	13.55 ± 0.46	17.45 ± 0.32	11.5 ± 0.5	0.25 ± 0.01

FIGURE 2 Hydrogel gelation kinetics and collagen structure visualization. Turbidity gelation kinetic graphs of (A) iPN and (B) collagen I hydrogels. Graphs were analyzed to determine the time until 50% gelation (t_{50}), 95% gelation (t_{95}), time until gelation is initiated (t_{lag}), and speed of gelation (s) or slope of the linear region on the graphs. Values are reported in (C) as mean ± SD. Confocal micrographs for fibrillar collagen formation in iPN (D) and collagen I (E) hydrogels were also obtained to visualize collagen fiber structure and confirm collagen fibrillogenesis gelling mechanism

not significantly different between 7.5 and 10 mg/ml samples (12.85 ± 0.27 min and 13.55 ± 0.46 min, respectively). When concentrations were compared between materials, 7.5 mg/ml iPN t_{50} was significantly longer than 7.5 mg/ml collagen I ($p < 0.05$). At 10 mg/ml, there was no significant difference in time to 50% gelation between iPN and collagen I samples.

The 7.5 mg/ml iPN hydrogels reached full gelation (t_{95}) significantly slower than 10 mg/ml iPN (17.44 ± 0.21 min vs. 15.68 ± 0.85 min, respectively) ($p < 0.05$). Collagen I hydrogels, however, experienced the opposite trend where the 7.5 mg/ml t_{95} was significantly lower than the t_{95} at 10 mg/ml (14.90 ± 0.26 min vs. 17.45 ± 0.32 min, respectively) ($p < 0.05$). Comparing across the materials, at 7.5 mg/ml, the iPN hydrogels took significantly longer to reach full gelation compared to collagen I ($p < 0.05$). However, this was the opposite for 10 mg/ml, where the iPN reached full gelation faster than collagen analogues ($p < 0.05$).

Speed of gelation (S) was found to be concentration independent. No significant differences between concentrations of a given material were found. Between materials, however, the iPN gelation speed was found to be significantly slower than the collagen I analogues for both concentrations ($p < 0.05$). Although there are significant differences in gelation parameters between concentrations and materials, gelation is still occurring in all samples in under 20 min. This duration should be an appropriate amount of time for easy handling during injection while still allowing for efficient encapsulation and delivery of desired drug or cells in vivo. The efficacy of this timing will need to be further assessed in future in vivo studies and could require partial gelation prior to injection.

3.3 | Visualization of iPN hydrogel microstructure

To support turbidity gelation kinetic findings, confocal reflectance was used to visualize fibrillar collagen structure and whether fibrillogenesis occurred. Representative confocal images are shown in Figure 2(D,E). Images reveal that extensive collagen fiber networks exist in both collagen I and iPN hydrogel samples. Given the turbidity gelation pattern/parameters and confocal reflectance data, it is likely that collagen I fibrillogenesis is the driving force behind iPN gelation.

3.4 | Mechanical characterization of iPN hydrogel

The compressive, viscoelastic, and rheological properties of iPN hydrogels were assessed to ensure that the iPN would provide a mechanical microenvironment comparable to neural tissue. Overall, iPN hydrogels were significantly softer than collagen I analogues. Steady-state compressive modulus (SSM) for iPN and collagen I hydrogels are shown in Figure 3(A). The 7.5 and 10 mg/ml iPN hydrogels each had significantly lower SSMs than collagen I hydrogels at 10 mg/ml concentration (159.9 ± 39.6 Pa and 196.7 ± 14.17 Pa for 7.5 and 10 mg/ml iPN, respectively, compared to 543.1 ± 46.4 Pa for 10 mg/ml collagen I). The characteristic time, an indication of material

viscoelasticity and relaxation speed,[75] was about 8–11 s for all samples not significantly different between any of the groups (Figure 3 (B)). Rheological properties (storage and loss modulus) were determined for iPN and collagen I hydrogels and results are shown in Figure 3(C,D). The trends found were identical to those of the SSM, with iPN hydrogels having significantly lower storage and loss moduli than collagen I analogues. Additionally, 10 mg/ml collagen I hydrogels had significantly higher loss and storage moduli than 7.5 mg/ml iPN and collagen I hydrogels. Overall, the compressive properties and rheological properties of the iPN hydrogels were within range of values reported for neural tissue in the literature,[76-81] suggesting that these iPN matrices would provide appropriate mechanical cues to both transplanted cell populations as well as regenerating axons.

## 3.5 | Degradation and swelling properties of iPN hydrogel

In vitro degradation was assessed to compare relative degradation rates of iPN to common collagen I hydrogels. Degradation profiles depicting cumulative mass loss of iPN and collagen I hydrogels are shown in Figure 4(A,B). Both concentrations of collagen I hydrogels had lost ~80% of the cumulative mass over the 30-day investigation. These degradation profiles were essentially linear ($R^2 = 0.95$ for 7.5 mg/ml and $R^2 = 0.98$ for 10 mg/ml). The iPN, however, experienced a faster degradation than analogous collagen I hydrogels with a significantly higher percent weight loss at representative time points 7, 15, and 30 days. Additionally, the degradation profile was less linear ($R^2 = 0.73$ for 7.5 mg/ml iPN and $R^2 = 0.87$ for 10 mg/ml iPN). By the end of the 30-day investigation, the 10 mg/ml iPN hydrogels had lost 95% of their weight and the 7.5 mg/ml iPN hydrogels were fully degraded. By 15 days into the investigation, the 7.5 mg/ml iPN hydrogels had almost entirely degraded.

The swelling capacities of iPN and collagen I hydrogels were measured to understand the ability of the materials to absorb water, which can affect other properties such as drug release[82,83] (Figure 4(C)). The swelling ratio of the two iPN hydrogel concentrations were not significantly different. Similarly, the swelling ratio was not significantly different between the two collagen I concentrations. However, the swelling ratio of both iPN concentrations was significantly greater than that of 10 mg/ml collagen I hydrogels, indicating greater swelling in the iPN hydrogels.

3.6 | Schwann cell in vitro biocompatibility

Since 7.5 and 10 mg/ml iPN hydrogels had largely similar mechanical properties and characteristics, only the 7.5 mg/ml concentrations of iPN and collagen I hydrogels were explored in subsequent in vitro studies.

Primary rat Schwann cells were cultured inside 7.5 mg/ml iPN and collagen I hydrogels for 3 days, after which alamarBlue metabolic
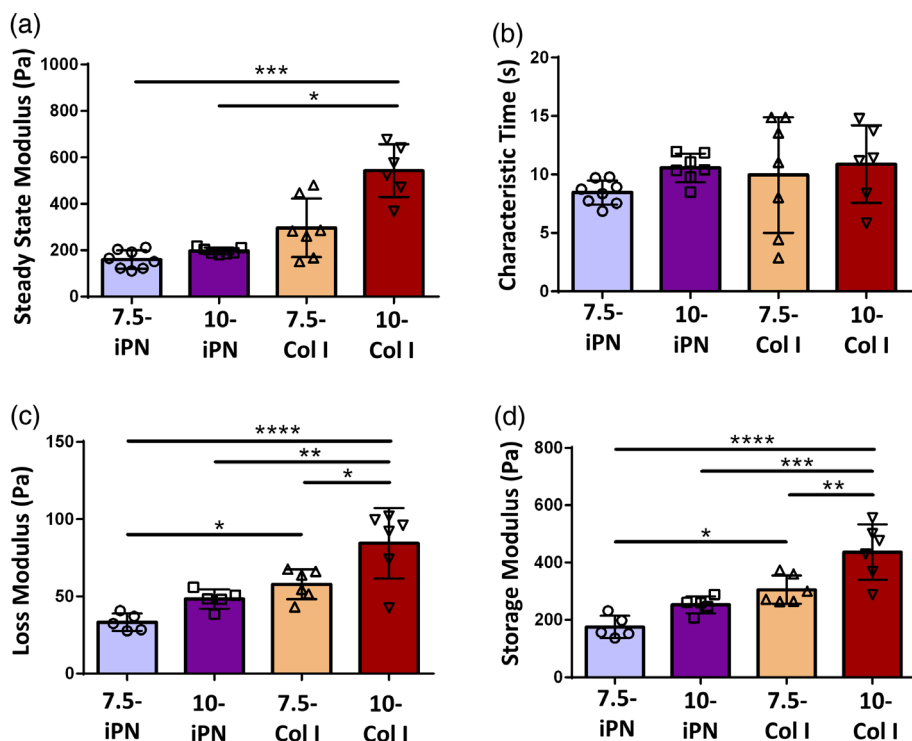
FIGURE 3 Mechanical characterization of iPN hydrogels. Mesoscale indentation was used to determine the (A) steady-state compressive modulus (SSM) and (B) characteristic time of 7.5 and 10 mg/ml iPN and collagen I (Col I) hydrogels. Rheological assessment was performed to determine the (C) loss and (D) storage moduli of iPN and collagen I hydrogels. Each data point represents one sample (one hydrogel). Data presented as mean ± SD. *$p < 0.05$, **$p < 0.01$, ***$p < 0.001$, ****$p < 0.0001$
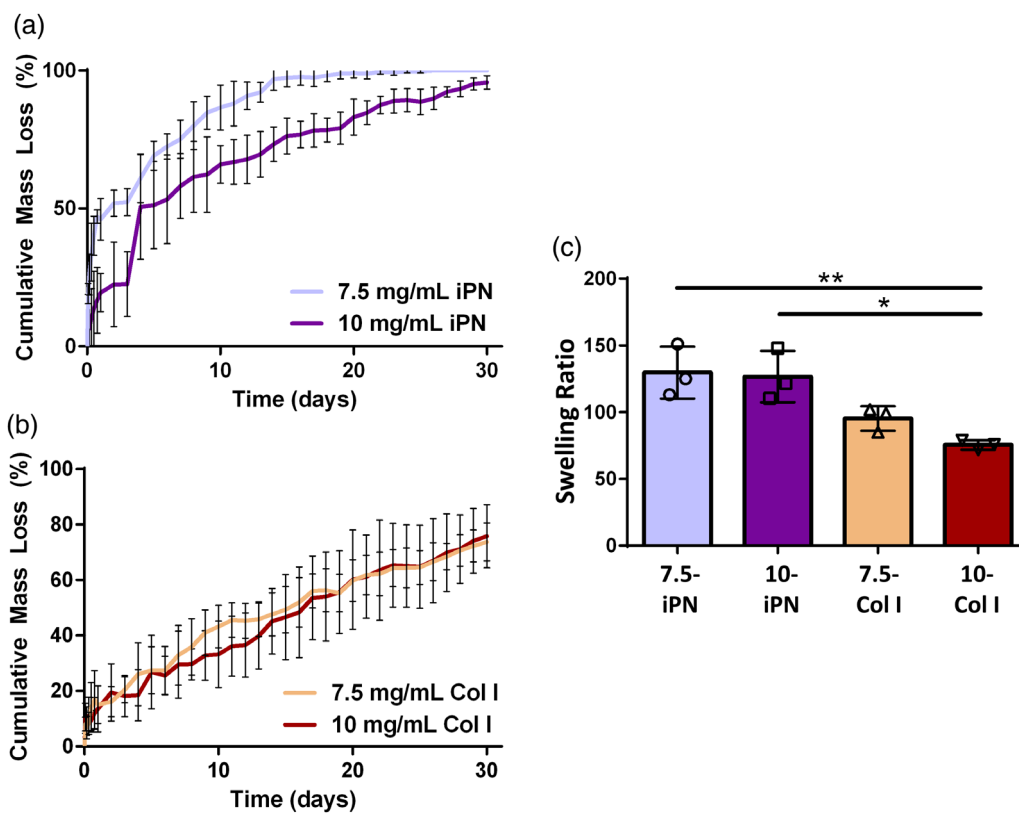

FIGURE 4 Hydrogel in vitro degradation and swelling properties. An in vitro degradation assessment was performed on 7.5 and 10 mg/ml (A) iPN and (B) collagen I (Col I) hydrogels, where degradation is depicted as cumulative mass loss (y-axis) over time (x-axis). The swelling ratios of iPN and collagen I hydrogels after 24 h were measured (C) and complement degradation rates. Data presented as mean ± SD. *$p < 0.05$, **$p < 0.01$

assay, live/dead staining, and confocal imaging were performed. Figure 5 displays representative images of live (green) and dead (red) cells present in the hydrogels. The confocal 3D-rendered images show that hydrogels remained intact after 3 days in culture. The number of live and dead cells were quantified in ImageJ and the percentage of live cells relative to total number of cells is represented in the graph in Figure 5(C). The average percent viability of Schwann cells was 83.7 ± 6.9% in collagen I hydrogels and 88.6 ± 3.9% in iPN hydrogels, with no significant difference detected between the two. Figure 5(B) depicts metabolic activity levels of Schwann cells cultured in the collagen I and iPN hydrogels. Each data point represents the fluorescence intensity of a unique sample normalized to the average of the collagen I samples. The average metabolic activity of Schwann cells in iPN hydrogels was 2.8% higher than that in collagen I hydrogels. However, no statistically significant differences were detected between groups.

3.7 | Astrocyte spreading within hydrogels

Astrocytes were grown inside of 7.5 mg/ml hydrogels to assess the effect of hydrogel material on cell spreading. Cells were cultured for 3 days, after which they were fixed, sectioned, and stained for glial fibrillary acidic protein (GFAP), which is an intermediate filament protein commonly used as a marker for astrocytes.[84] Representative images of astrocytes in each group can be seen in Figure 6(A). It is evident that astrocytes grown in the collagen I hydrogels did not form many processes compared to those cultured in iPN. To quantify this phenotype, the average area covered by each astrocyte was calculated using ImageJ, and these values are shown in Figure 6(B). On average, astrocytes covered about twice the area in iPN hydrogels compared to collagen hydrogels (p-value < 0.01 between iPN and collagen hydrogels). The average circularity of astrocytes was also calculated in ImageJ and these values are shown in Figure 6(C). The average circularity, or roundness, of astrocytes in collagen hydrogels was 0.677 ± 0.051, compared to 0.615 ± 0.022 in iPN hydrogels, where a value of 1 is a perfect circle and 0 is an elongated polygon. The differences in circularity between the two groups were statistically significant ($p < 0.05$). A decrease in roundness should indicate better cell spreading in the biomaterial,[85] which was confirmed by the correlation of results between the percent area covered and cell shape. Overall, results indicate that the iPN hydrogel at this concentration may be more suitable for supporting astrocyte adhesion and growth.
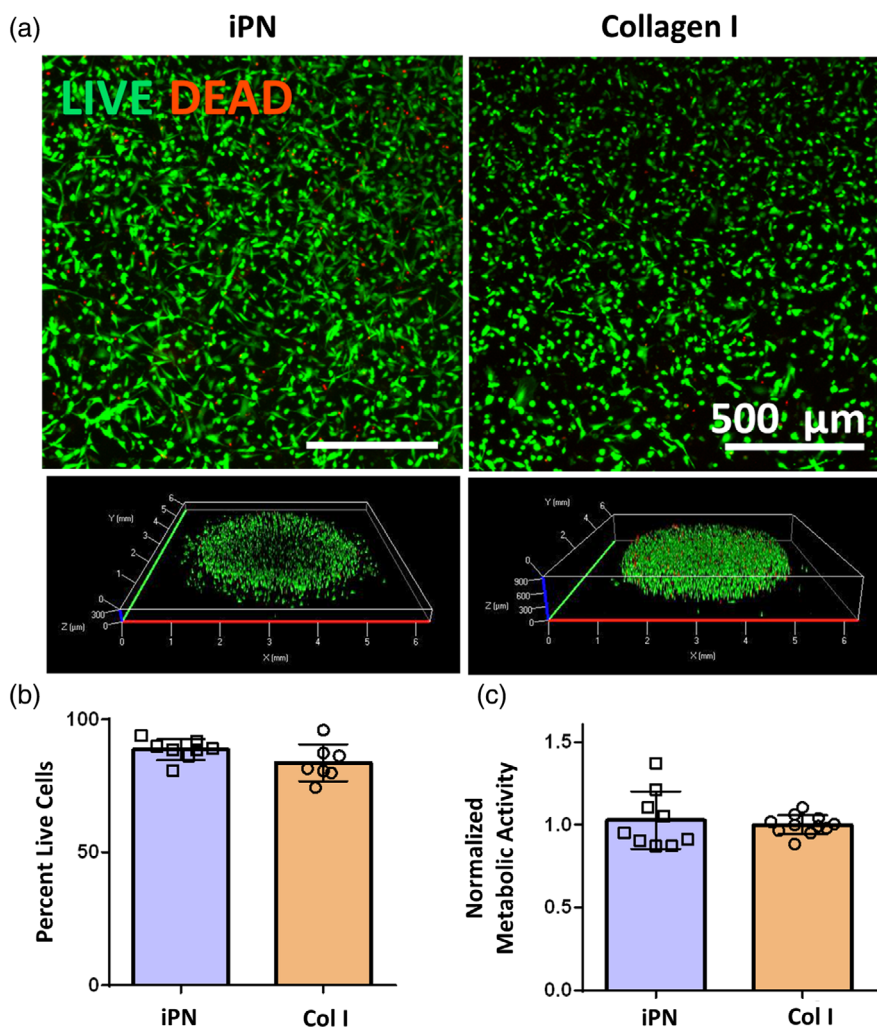
FIGURE 5 In vitro biocompatibility of Schwann cells cultured in 7.5 mg/ml iPN and collagen I hydrogels. (A) Representative 2D images (top) and 3D-rendered images of live (green) and dead (red) Schwann cells. (B) Percentage of live Schwann cells after 3 days of culture in hydrogels, as quantified with ImageJ. (C) Graph of normalized metabolic activity of Schwann cells as determined by an alamarBlue assay. Each data point represents one sample (one hydrogel). Data presented as mean ± SD
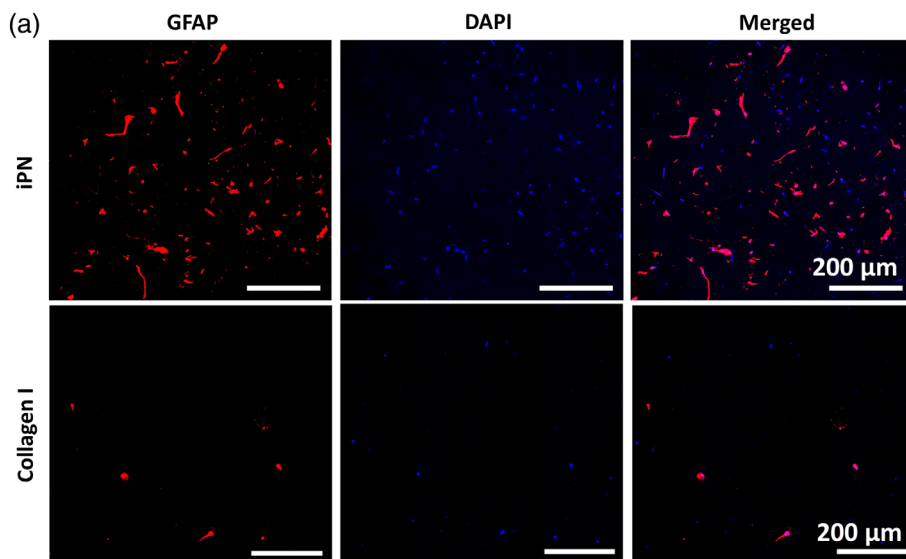
FIGURE 6 Astrocytes in 7.5 mg/ml hydrogels stained with GFAP (red) for astrocytes and DAPI (blue) for nuclei. (A) Representative images of astrocytes cultured in iPN and collagen I 7.5 mg/ml hydrogels. (B) Semi-quantification of the average area covered per astrocyte in each hydrogel. (C) Average circularity of astrocytes inside each hydrogel. Data presented as mean ± SD. *$p < 0.05$, **$p < 0.01$
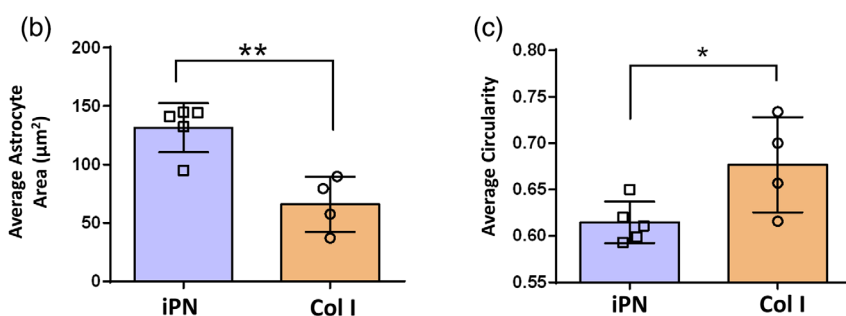
3.8 | FITC-dextran in vitro release kinetics

Elution studies were performed in vitro to determine the release profile of 20 kDa FITC-dextran from the iPN hydrogel. This molecule was chosen for its similar molecular weight to neurotrophic factors such as brain-derived neurotrophic factor (BDNF) and glial cell line-derived neurotrophic factor (GDNF).[86,87] FITC-dextran was incorporated into iPN pre-gel solution and incubated at 37°C to form hydrogels. Hydrogels were placed in a well plate and submerged in PBS, then placed on a shaker plate at 37°C. Eluates were collected at various time points up to 48 h. Almost 90% of FITC-dextran had been released after 6 h of incubation (Figure 7), and about 98% had been released after 48 h, hence no further eluates were collected.

From these data, it was clear that an additional technique was needed to obtain a more sustained release of "drug" from the iPN hydrogel. Polylactic-co-glycolic acid (PLGA) is an attractive polymer for drug delivery applications because it is biodegradable and biocompatible, has been previously approved by the FDA for drug delivery systems, and is capable of encapsulating either hydrophilic or hydrophobic drugs and small molecule therapeutics to protect them from degradation.[88] Further, encapsulating drugs in PLGA nano- or microparticles can slow the degradation of the drug and hence provide a sustained, rather than burst, release, while decreasing dosing frequency.[89] Thus, PLGA microparticles were explored as a complementary approach to control the release of desired biomolecules. To
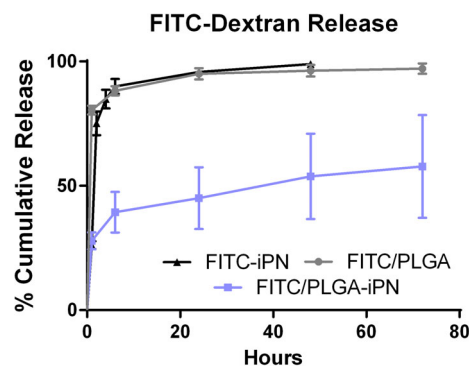
FIGURE 7 FITC-dextran release from iPN 7.5 mg/ml hydrogels. Cumulative release of FITC-dextran alone from iPN hydrogels (FITC-iPN), from FITC-dextran-loaded PLGA microparticles incorporated into iPN hydrogels (FITC/PLGA-iPN), and from FITC-dextran-loaded PLGA microparticles suspended in PBS (FITC/PLGA). The combination of PLGA encapsulation as well as incorporation into the iPN hydrogel successfully sustains the release of FITC-dextran over at least 3 days. Experimental time points were 1, 6, 24, 48, and 72 h. Data presented as mean ± SD

determine the range of release times, FITC-dextran, a model compound as noted above, was encapsulated in PLGA microparticles (information on particle size and loading efficiency can be found in the methodology section and supplementary data S1). FITC-PLGA particles were then incorporated into iPN hydrogels, and the same

elution experiment was performed, with control groups of free-floating FITC-PLGA particles and blank PLGA particles. The eluates were collected over 72 h. Compared to the free particles and FITC-dextran alone, it is clear that the iPN delays the release of FITC-dextran considerably (Figure 7). For example, at any given time point, the amount of FITC-dextran released from free particles is more than half of that released from particles encapsulated in the iPN hydrogels.

4 | DISCUSSION

In this work, we have optimized the solubilization of decellularized nerve scaffolds, processed using a new sodium deoxycholate and DNase (SDD) decellularization method,[50] and demonstrated that iPN scaffolds can be successfully generated and have attractive properties for neural repair strategies. Previous work has utilized iPN hydrogels derived from Hudson method-decellularized nerves.[48] However, as this protocol is now obsolete,[50] it was necessary to generate iPN from SDD decellularized nerves. We successfully solubilized SDD-decellularized nerves and formed injectable, in situ gelling hydrogels at tissue concentrations of 7.5 and 10 mg decellularized tissue per ml of pepsin/HCl solution. After qualitatively assessing gelation, it was important to better understand gelation parameters and mechanical properties.

Gelation parameters, such as time to full gelation, are useful to understand for injectable therapies so that efflux of the pre-gel solution out of the lesion or injury site is minimized.[20] First, we assessed turbidity gelation kinetics. In this method, gelation is determined by collagen fibrillogenesis. iPN scaffolds were observed to exhibit the signature sigmoidal gelation kinetic profile of collagen I-based materials.[90-92] This sigmoidal profile was expected, as collagen I is known to be one of the most abundant ECM molecules in peripheral nerve.[93-95] Similarity in gelation kinetic profiles strongly suggested that the gelation of iPN was a result of collagen fibril formation. The presence of collagen fibril formation was further confirmed by confocal reflectance. Both iPN and collagen I samples formed hydrogels in under 20 min, and all types of samples formed hydrogels within 5 min of each other. However, one notable difference between iPN and collagen controls was the lag time until gelation was initiated. The longer lag time observed in the iPN hydrogels is most likely due to the other non-fibrillar ECM proteins, such as laminin and collagen IV, which have been shown to impede collagen I fibrillogenesis relative to pure collagen I samples.[90,96,97] In general, gelation time should be minimized to reduce leakage of the material out of the injury site and sedimentation of suspended components (i.e., transplanted cells).[20,71] Despite the longer lag time compared to collagen I, the iPN hydrogel formed in less than 20 min. This seems to be an acceptable duration based on the literature,[71] however needs further exploration in vivo.

Matching the approximate mechanical properties of target tissue is important because these properties can drive cellular behavior, including neurite outgrowth.[16,18-20] The mechanical microenvironment also should closely match that of the target tissue as to not cause additional injury or inflammatory responses.[21-26] Mesoscale indentation was employed to determine compressive and viscoelastic properties of the iPN hydrogels,[55,75,98] and rheological assessment was performed to assess the storage and loss moduli. Compressive modulus values of brain, spinal cord, and peripheral nerve are reported between 50 Pa and 7 kPa.[55,56,76-79,99] These values are highly dependent on methodology, orientation of the spinal cord, donor species and age, and presence of dura mater. In literature, storage moduli for CNS tissue ranges from 150 Pa to 5 kPa and loss moduli ranging from 40 to 1000 Pa at frequencies equal to or under 10 Hz (similar to this investigation).[80,81] Compressive and rheological data together demonstrate that the material properties of the iPN are within the range of neural tissues reported in literature.[76-79] Further, multiple studies suggest a stiffness of ~50–250 Pa promotes significantly more neurite outgrowth compared to softer (~10 Pa) and stiffer substrates (> 330 Pa).[80,100-102] Both concentrations of iPN have properties near this ideal range and may suggest the iPN can better encourage regeneration after neural injury compared to stiffer hydrogels, such as the collagen I controls.

Hydrogels are materials that will swell in an aqueous environment like in vivo conditions.[12-14] Determining the swelling capacity in vitro can provide information to help determine, for example, how much material to inject into the spinal cord or brain such that the material does not impart excessive pressure on the damaged tissue.[11,103] Additionally, the swelling properties of a hydrogel are directly related to other important characteristics, such as diffusivity and drug release.[82,83] The iPN hydrogel swelling ratios determined are within range of other natural polymer hydrogels that are used for SCI and peripheral nerve injury repair.[11,104] To the best of our knowledge, swelling properties of iPN have not been investigated previously.

Determining the in vitro degradation rate of a biomaterial scaffold can provide useful information regarding how long the scaffold will last without cellular influence. In vitro degradation studies suggested that in vivo degradation of iPN (without deposition of new ECM by transplanted cells) would be approximately 1 month or less because of native enzyme presence. Compared to collagen I controls, the iPN materials experienced increased degradation, especially within the first week. This may reflect the loss of loosely associated non-fibrillar proteins from the hydrogel. The degradation profile determined in this study was limited, as there were no proteases or cellular influence. In vivo, it is likely that the iPN hydrogels will degrade at a faster rate. However, if the iPN is used to deliver bioactive molecules, it is likely that the molecules would be released or become inactive by the time the hydrogel fully degrades, deeming the hydrogel degradation profile acceptable.

It was determined that Schwann cell viability was greater than 80% in both 7.5 mg/ml iPN and collagen I hydrogels, suggesting that the iPN is a biocompatible material based on previous materials that have been immunologically tolerated in vivo.[49] Furthermore, there was no detected difference in the metabolic activity of Schwann cells cultured in either material. These results also demonstrate that the iPN could be a potential delivery vehicle for cell-based therapies.

Astrocytes cultured inside iPN hydrogels more readily spread out and formed processes than those cultured inside collagen I hydrogels. ImageJ semi-quantification also demonstrated a significantly increased area covered by astrocytes as well as decreased circularity in iPN

hydrogels compared to collagen I hydrogels. It should be noted that fewer cells, in general, were seen in collagen hydrogel sections compared to iPN hydrogel sections, even though the same number of cells were initially seeded in all hydrogels. This higher density of cells observed could indicate that the iPN hydrogel better supports astrocyte adhesion and growth, hence better survival through the culture and processing conditions. These astrocyte spreading results are promising, as astrocytes play an important role in regeneration after CNS injury by migrating to compact the lesion center, isolating the injury site to reduce the spread of inflammatory cells and their cytotoxic by-products, and restoring homeostasis.[2,105,106] Although activated astrocytes are traditionally associated with formation of glial scar after traumatic spinal cord and brain injury, which creates an obstacle for neural regeneration,[107] recent studies have actually shown that the presence of astrocytes themselves, even in a scarring context, are necessary for axon regeneration as they express a multitude of factors that support axonal growth.[108] Future studies could include assessment of astrocyte spreading and cell-material interaction over longer periods of time. Additionally, it would be useful to understand how other neural cell populations, in particular neurons, respond to the iPN hydrogel. Future experiments will more thoroughly focus on in vitro assessments of nerve regeneration, and eventually in vivo biocompatibility and efficacy.

The iPN hydrogel's injectability allows it to serve as a delivery vehicle for different combinatorial neural repair strategies. If the iPN may be combined with pharmaceutical approaches, it is important to understand release profiles for compounds from the material. To preliminarily understand drug release from iPN hydrogels, FITC-dextran of a comparable size to neurotrophic factors used in neural injury repair[109-111] (20 KDa) was loaded into the iPN and its release was measured over time. The iPN hydrogels experienced a burst release of almost 90% of the loaded FITC-dextran within the first 6 h. It is likely that release of actual growth factors would be delayed, as the ECM has been shown to sequester and bind to growth factors.[112-114] However, to achieve more regulated and sustained release, encapsulation in PLGA microparticles was employed. A three-day elution study was performed on FITC-dextran-loaded PLGA microparticles encapsulated in iPN hydrogels. It was found that the amount of FITC-dextran released at any given time point was less than half that of free FITC-dextran or free-floating particle controls. Although FITC-dextran is similar in size to neurotrophic factors, it is possible that such factors are more difficult to encapsulate and assess due to low in vivo stability.[115,116] Future studies will focus on encapsulation and release of neurotrophic factors such as BDNF and GDNF, and their physiological effects in vitro and in vivo. However, the work thus far shows promise for the use of iPN hydrogels in combinatorial therapies for neural injuries.

5 | CONCLUSION

In this work, we have demonstrated that injectable, thermally gelling hydrogels have successfully been fabricated from a reoptimized, novel decellularization process (SDD method) that has been shown to preserve ECM and remove cellular content. The iPN hydrogels form in under 20 min and have mechanical properties similar to native neural tissue. The in vitro biocompatibility of the iPN hydrogels has been demonstrated through Schwann cell viability experiments. Additionally, iPN hydrogels promote greater astrocyte spreading compared to collagen I hydrogels, demonstrating that the iPN possesses potential advantages over collagen I hydrogels for neural cell growth. Finally, the iPN is a promising delivery vehicle of drug-loaded microparticles for a combinatorial approach to neural injury therapies. Overall, iPN hydrogels generated from SDD method decellularized nerves represent a promising biocompatible platform for development of novel, multi-faceted therapies for neural injury repair.

CONFLICT OF INTEREST
The authors declare no conflicts of interest.

DATA AVAILABILITY STATEMENT
The data that support the findings of this study are available from the corresponding author upon reasonable request.

ORCID
Deanna Bousalis 🔟 https://orcid.org/0000-0002-6085-9250

REFERENCES
1. Amani H, Kazerooni H, Hassanpoor H, Akbarzadeh A, Pazoki-Toroudi H. Tailoring synthetic polymeric biomaterials towards nerve tissue engineering: a review. *Artif Cells Nanomed Biotechnol*. 2019; 47:3524-3539. https://doi.org/10.1080/21691401.2019.1639723
2. Ahuja CS, Wilson JR, Nori S, et al. Traumatic spinal cord injury. *Nat Rev Dis Primers*. 2017;3:7018.
3. Bradbury EJ, Burnside ER. Moving beyond the glial scar for spinal cord repair. *Nat Commun*. 2019;10:3879. https://doi.org/10.1038/s41467-019-11707-7
4. Belanger K, Dinis TM, Taourirt S, Vidal G, Kaplan DL, Egles C. Recent strategies in tissue engineering for guided peripheral nerve regeneration. *Macromol Biosci*. 2016;16:472-481. https://doi.org/10.1002/mabi.201500367
5. Kasper M, Deister C, Beck F, Schmidt CE. Bench-to-bedside lessons learned: commercialization of an acellular nerve graft. *Adv Healthc Mater*. 2020;9:174. https://doi.org/10.1002/adhm.202000174
6. Funnell JL, Balouch B, Gilbert RJ. Magnetic composite biomaterials for neural regeneration. *Front Bioeng Biotechnol*. 2019;7. https://doi.org/10.3389/fbioe.2019.00179
7. Lacko CS, Singh, I, Wall, MA, et al. Magnetic particle templating of hydrogels: engineering naturally derived hydrogel scaffolds with 3D aligned microarchitecture for nerve repair. *J Neural Eng*. 2020;17. https://doi.org/10.1088/1741-2552/ab4a22
8. Vijayavenkataraman S. Nerve guide conduits for peripheral nerve injury repair: a review on design, materials and fabrication methods. *Acta Biomater*. 2020;106:54-69. https://doi.org/10.1016/j.actbio.2020.02.003
9. Hlavac N, Kasper M, Schmidt CE. Progress toward finding the perfect match: hydrogels for treatment of central nervous system injury. *Mater Today Advan*. 2020;6:39. https://doi.org/10.1016/j.mtadv.2019.100039

10. Côté M-P, Amin AA, Tom VJ, Houle JD. Peripheral nerve grafts support regeneration after spinal cord injury. *Neurotherapeutics*. 2011;8: 294-303.

11. Khaing ZZ, Ehsanipour A, Hofstetter CP, Seidlits SK. Injectable hydrogels for spinal cord repair: a focus on swelling and intraspinal pressure. *Cells Tissues Organs*. 2016;202:67-84.

12. Chai Q, Jiao Y, Yu X. Hydrogels for biomedical applications: their characteristics and the mechanisms behind them. *Gels*. 2017;3:6.

13. Ahmed E, Hydrogel M. Preparation, characterization, and applications: a review. *J Adv Res*. 2015;6:105-121.

14. Bahram M, Mohseni N, Moghtader M. An introduction to hydrogels and some recent applications. *Emerging Concepts in Analysis and Applications of Hydrogels*. United Kingdom: InTech; 2016. https:// doi.org/10.5772/64301

15. Straley KS, Foo CWP, Heilshorn SC. Biomaterial design strategies for the treatment of spinal cord injuries. *J Neurotrauma*. 2010;27:1-19.

16. Wang M, Zhai P, Chen X, Schreyer DJ, Sun X, Cui F. Bioengineered scaffolds for spinal cord repair. *Tissue Eng Part B Rev*. 2011;17: 177-194.

17. Perale G, Rossi F, Sundstrom E, et al. Hydrogels in spinal cord injury repair strategies. *ACS Chem Nerosci*. 2011;2:336-345.

18. Führmann T, Anandakumaran PN, Shoichet MS. Combinatorial therapies after spinal cord injury: how can biomaterials help? *Adv Healthc Mater*. 2017;6(10).

19. Assunção-Silva RC, Gomes ED, Sousa N, Silva NA, Salgado AJ. Hydrogels and cell based therapies in spinal cord injury regeneration. *Stem Cells Int*. 2015;2015:1-24.

20. Macaya D, Spector M. Injectable hydrogel materials for spinal cord regeneration: a review. *Biomed Mater*. 2012;7:2001.

21. Carnicer-Lombarte A, Barone, DG, Dimov, IB, et al. Mechanical matching of implant to host minimises foreign body reaction. *Bioarxiv*. 2019;648. https://doi.org/10.1101/829648

22. Seifu DG, Purnama A, Mequanint K, Mantovani D. Small-diameter vascular tissue engineering. *Nat Rev Cardiol*. 2013;10:410-421.

23. Lind G, Linsmeier CE, Schouenborg J. The density difference between tissue and neural probes is a key factor for glial scarring. *Sci Rep*. 2013;3:2942.

24. Green RA, Lovell NH, Wallace GG, Poole-Warren LA. Conducting polymers for neural interfaces: challenges in developing an effective long-term implant. *Biomaterials*. 2008;29:3393-3399.

25. Feig VR, Tran H, Lee M, Bao Z. Mechanically tunable conductive interpenetrating network hydrogels that mimic the elastic moduli of biological tissue. *Nat Commun*. 2018;9:2740.

26. Prodanov D, Delbeke J. Mechanical and biological interactions of implants with the brain and their impact on implant design. *Front Neurosci*. 2016;10.

27. Haggerty AE, Oudega M. Biomaterials for spinal cord repair. *Neurosci Bull*. 2013;29:445-459.

28. Prest TA, Yeager E, LoPresti ST, et al. Nerve-specific, xenogeneic extracellular matrix hydrogel promotes recovery following peripheral nerve injury. *J Biomed Mater Res Part A*. 2018;106:450-459. https:// doi.org/10.1002/jbm.a.36235

29. Kohn-Polster C, Bhatnagar D, Woloszyn D, et al. Dual-component gelatinous peptide/reactive oligomer formulations as conduit material and luminal filler for peripheral nerve regeneration. *Int J Mol Sci*. 2017;18(5):1104. https://doi.org/10.3390/ijms18051104

30. Gros T, Sakamoto JS, Blesch A, Havton LA, Tuszynski MH. Regeneration of long-tract axons through sites of spinal cord injury using templated agarose scaffolds. *Biomaterials*. 2010;31:6719-6729. https://doi.org/10.1016/j.biomaterials.2010.04.035

31. Carriel V, Garrido-Gómez J, Hernández-Cortés P, et al. Combination of fibrin-agarose hydrogels and adipose-derived mesenchymal stem cells for peripheral nerve regeneration. *J Neural Eng*. 2013;10:6022. https://doi.org/10.1088/1741-2560/10/2/026022

32. Mothe AJ, Tam RY, Zahir T, Tator CH, Shoichet MS. Repair of the injured spinal cord by transplantation of neural stem cells in a hyaluronan-based hydrogel. *Biomaterials*. 2013;34:3775-3783. https://doi.org/10.1016/j.biomaterials.2013.02.002

33. Khaing ZZ, Agrawal NK, Park JH, et al. Localized and sustained release of brain-derived neurotrophic factor from injectable hydrogel/microparticle composites fosters spinal learning after spinal cord injury. *J Mater Chem B*. 2016;7560:7560-7571.

34. Gupta D, Tator CH, Shoichet MS. Fast-gelling injectable blend of hyaluronan and methylcellulose for intrathecal, localized delivery to the injured spinal cord. *Biomaterials*. 2006;27:2370-2379. https:// doi.org/10.1016/j.biomaterials.2005.11.015

35. Taylor SJ, McDonald JW, Sakiyama-Elbert SE. Controlled release of neurotrophin-3 from fibrin gels for spinal cord injury. *J Control Release*. 2004;98:281-294. https://doi.org/10.1016/j.jconrel.2004. 05.003

36. Ansorena E, de Berdt P, Ucakar B, et al. Injectable alginate hydrogel loaded with GDNF promotes functional recovery in a hemisection model of spinal cord injury. *Int J Pharm*. 2013;455:148-158. https://doi.org/10.1016/j.ijpharm.2013.07.045

37. Suzuki Y, Ishikawa N, Tanihara M, Saito S. Nontubulation repair of peripheral nerve gap using heparin/alginate gel combined with b-FGF. *Plast Reconstr Surg Glob Open*. 2016;4:600. https://doi.org/10. 1097/GOX.0000000000000581

38. Tsai EC, Dalton PD, Shoichet MS, Tator CH. Matrix inclusion within synthetic hydrogel guidance channels improves specific supraspinal and local axonal regeneration after complete spinal cord transection. *Biomaterials*. 2006;27:519-533. https://doi.org/10.1016/j.bioma terials.2005.07.025

39. Vijayavenkataraman S, Vialli N, Fuh JYH, Lu WF. Conductive collagen/polypyrrole-b-polycaprolactone hydrogel for bioprinting of neural tissue constructs. *Int J Bioprint*. 2019;5(2.1). https://doi.org/ 10.18063/ijb.v5i2.1.229

40. Madduri S, Feldman K, Tervoort T, Papaloïzos M, Gander B. Collagen nerve conduits releasing the neurotrophic factors GDNF and NGF. *J Control Release*. 2010;143:168-174. https://doi.org/10.1016/j. jconrel.2009.12.017

41. Hopkins AM, de Laporte L, Tortelli F, et al. Silk hydrogels as soft substrates for neural tissue engineering. *Adv Funct Mater*. 2013;23: 5140-5149. https://doi.org/10.1002/adfm.201300435

42. Ahuja CS, Fehlings M. Concise review: bridging the gap: novel neuroregenerative and neuroprotective strategies in spinal cord injury. *Stem Cells Transl Med*. 2016;5:914-924. https://doi.org/10.5966/ sctm.2015-0381

43. Cheng TY, Chen MH, Chang WH, Huang MY, Wang TW. Neural stem cells encapsulated in a functionalized self-assembling peptide hydrogel for brain tissue engineering. *Biomaterials*. 2013;34:2005-2016. https://doi.org/10.1016/j.biomaterials.20 12.11.043

44. Saldin LT, Cramer MC, Velankar SS, White LJ, Badylak SF. Extracellular matrix hydrogels from decellularized tissues: structure and function. *Acta Biomater*. 2017;49:1-15.

45. Spang MT, Christman KL. Extracellular matrix hydrogel therapies: in vivo applications and development. *Acta Biomater*. 2018;68:1-14. https://doi.org/10.1016/j.actbio.2017.12.019

46. Hong JY, Seo Y, Davaa G, Kim HW, Kim SH, Hyun JK. Decellularized brain matrix enhances macrophage polarization and functional improvements in rat spinal cord injury. *Acta Biomater*. 2020;101: 357-371. https://doi.org/10.1016/j.actbio.2019.11.012

47. Hudson TW, Liu SY, Schmidt CE. Engineering an improved acellular nerve graft via optimized chemical processing. *Tissue Eng*. 2004;10: 1346-1358.

48. Cornelison RC, Gonzalez-Rothi EJ, Porvasnik SL, et al. Injectable hydrogels of optimized acellular nerve for injection in the injured

spinal cord. *Biomed Mater*. 2018;13:110. https://doi.org/10.1088/1748-605X/aaab82

49. Cerqueira SR, Lee YS, Cornelison RC, et al. Decellularized peripheral nerve supports Schwann cell transplants and axon growth following spinal cord injury. *Biomaterials*. 2018;177:176-185.

50. McCrary MW, Vaughn NE, Hlavac N, Song YH, Wachs RA, Schmidt CE. Novel sodium deoxycholate-based chemical decellularization method for peripheral nerve. *Tissue Eng Part C Meth*. 2020;26:23-36. https://doi.org/10.1089/ten.tec.2019.0135

51. Liu X, Zheng C, Luo X, Wang X, Jiang H. Recent advances of collagen-based biomaterials: multi-hierarchical structure, modification and biomedical applications. *Mater Sci Eng C*. 2019;99:1509-1522. https://doi.org/10.1016/j.msec.2019.02.070

52. Zhong J, Chan A, Morad L, Kornblum HI, Guoping F, Carmichael ST. Hydrogel matrix to support stem cell survival after brain transplantation in stroke. *Neurorehabil Neural Repair*. 2010;24:636-644. https://doi.org/10.1177/1545968310361958

53. Yao L, de Ruiter GCW, Wang H, et al. Controlling dispersion of axonal regeneration using a multichannel collagen nerve conduit. *Biomaterials*. 2010;31:5789-5797. https://doi.org/10.1016/j.biomaterials.2010.03.081

54. Medberry, C. J., Crapo P. M., Siu B. F., Carruthers C. A., Wolf M. T., Nagarkar S. P., Agrawal V., Jones K. E., Kelly J., Johnson S. A., Velankar S. S., Watkins S. C., Modo M., Badylak S. F. Hydrogels derived from central nervous system extracellular matrix (2012). doi:https://doi.org/10.1016/j.biomaterials.2012.10.062, 34, 1033, 1040

55. Spearman BS, Agrawal NK, Rubiano A, Simmons CS, Mobini S, Schmidt CE. Tunable methacrylated hyaluronic acid-based hydrogels as scaffolds for soft tissue engineering applications. *J Biomed Mater Res Part A*. 2020;108:279-291.

56. Stewart DC, Rubiano A, Dyson K, Simmons CS. Mechanical characterization of human brain tumors from patients and comparison to potential surgical phantoms. *PLoS One*. 2017;12:7561. https://doi.org/10.1371/journal.pone.0177561

57. Johnson, K. L. Contact mechanics (1989). doi:https://doi.org/10.1201/b17110-2.

58. G G, F F. Hertz's miscellaneous papers. *Nature*. 1896;55:6-9. https://doi.org/10.1038/055006f0

59. Cowin, S. C. & Doty, S. B. Tissue mechanics. (2007). doi:https://doi.org/10.1007/978-0-387-49985-7

60. J T, J C, J G, Q W, H F. Construction and evaluation of fibrillar composite hydrogel of collagen/konjac glucomannan for potential biomedical applications. *Regen Biomater*. 2018;5:239-250.

61. S T, E M, A A, A K, S T. Plate-shape carbonated hydroxyapatite/collagen nanocomposite hydrogel via in situ mineralization of hydroxyapatite concurrent with gelation of collagen at pH = 7.4 and 37°C. *J Biomed Mater Res B Appl Biomater*. 2019;107:1920-1929.

62. Yang C. Enhanced physicochemical properties of collagen by using EDC/NHS-crosslinking. *Bull Mater Sci*. 2012;35:913-918.

63. Caliari SR, Burdick JA. A practical guide to hydrogels for cell culture. *Nat Methods*. 2016;13:405-414.

64. Fernandes-Cunha GM, Chen, KM, Chen, F, et al. In situ-forming collagen hydrogel crosslinked via multi-functional PEG as a matrix therapy for corneal defects. *Sci Rep*. 2020;10(101):1-13.

65. Camci-Unal G, Cuttica D, Annabi N, Demarchi D, Khademhosseini A. Synthesis and characterization of hybrid hyaluronic acid-gelatin hydrogels. *Biomacromolecules*. 2013;14:1085-1092.

66. Tsintou M, Dalamagkas K, Seifalian A. Injectable hydrogel versus plastically compressed collagen scaffold for central nervous system applications. *Int J Biomater*. 2018;2018:1-10.

67. Schmitt T, Kajave, N, Cai, H, et al. In vitro characterization of xeno-free clinically relevant human collagen and its applicability in cell-laden 3D bioprinting. *J Biomater Appl*. 2021;35:912-923.

68. Hlavac N, VandeVord PJ. Astrocyte mechano-activation by high-rate overpressure involves alterations in structural and junctional proteins. *Front Neurol*. 2019;10. https://doi.org/10.3389/fneur.2019.00099

69. Schildge S, Bohrer C, Beck K, Schachtrup C. Isolation and culture of mouse cortical astrocytes. *J Vis Exp*. 2013;71. https://doi.org/10.3791/50079

70. Antoine EE, Vlachos PP, Rylander MN. Review of collagen I hydrogels for bioengineered tissue microenvironments: characterization of mechanics, structure, and transport. *Tissue Eng Part B Rev*. 2014;20:683-696. https://doi.org/10.1089/ten.teb.2014.0086

71. Kornev VA, Grebenik EA, Solovieva AB, Dmitriev RI, Timashev PS. Hydrogel-assisted neuroregeneration approaches towards brain injury therapy: a state-of-the-art review. *Comput Struct Biotechnol J*. 2018;16:488-502.

72. Zhu J, Kaufman LJ. Collagen I self-assembly: revealing the developing structures that generate turbidity. *Biophys J*. 2014;106:1822-1831.

73. Parkinson J, Kadler KE, Brass A. Simple physical model of collagen fibrillogenesis based on diffusion limited aggregation. *J Mol Biol*. 1995;247:823-831. https://doi.org/10.1016/S0022-2836(05)80157-3

74. Fratzl, P. Collagen: structure and mechanics. (2008). doi:https://doi.org/10.1007/978-0-387-73906-9

75. Rubiano A, Galitz C, Simmons CS. Mechanical characterization by mesoscale indentation: advantages and pitfalls for tissue and scaffolds. *Tissue Eng Part C Meth*. 2019;25:619-629. https://doi.org/10.1089/ten.tec.2018.0372

76. Shetye SS, Troyer KL, Streijger F, et al. Nonlinear viscoelastic characterization of the porcine spinal cord. *Acta Biomater*. 2014;10:792-797.

77. Koser DEE, Moeendarbary E, Hanne J, Kuerten S, Franze K. CNS cell distribution and axon orientation determine local spinal cord mechanical properties. *Biophys J*. 2015;108:2137-2147.

78. Ozawa H, Matsumoto T, Ohashi T, Sato M, Kokubun S. Comparison of spinal cord gray matter and white matter softness: measurement by pipette aspiration method. *J Neurosurg*. 2001;95:221-224.

79. McKee CT, Last JA, Russell P, Murphy CJ. Indentation versus tensile measurements of Young's modulus for soft biological tissues. *Tissue Eng Part B Rev*. 2011;17:155-164.

80. Flanagan LA, Ju Y-E, Marg B, Osterfield M, Janmey PA. Neurite branching on deformable substrates. *Neuroreport*. 2002;13:2411-2415.

81. Chatelin S, Constantinesco A, Willinger R. Fifty years of brain tissue mechanical testing: from in vitro to in vivo investigations. *Biorheology*. 2010;47:255-276.

82. Ganji F, Vasheghani-Farahani S, Vasheghani-Farahani E. Theoretical description of hydrogel swelling: a review. *Iran Polym J*. 2010;19(5):375-398.

83. Kim SW, Bae YH, Okano T. Hydrogels: swelling, drug loading, and release. *Pharmaceut Res*. 1992;09:283-290. https://doi.org/10.1023/A:1015887213431

84. Middeldorp J, Hol EM. GFAP in health and disease. *Prog Neurobiol*. 2011;93:421-443. https://doi.org/10.1016/j.pneurobio.2011.01.005

85. Sriphutkiat Y, Kasetsirikul S, Ketpun D, Zhou Y. Cell alignment and accumulation using acoustic nozzle for bioprinting. *Sci Rep*. 2019;9:17774. https://doi.org/10.1038/s41598-019-54330-8

86. Recombinant human GDNF. Available at: https://www.peprotech.com/en/recombinant-human-gdnf.

87. Brain-Derived Neurotrophic Factor (BDNF). Available at: https://www.creativebiomart.net/therapeutic-proteins/p/238/brain-derived-neurotrophic-factor-bdnf/.

88. Danhier F, Ansorena E, Silva JM, Coco R, le Breton A, Préat V. PLGA-based nanoparticles: an overview of biomedical applications. *J Control Release*. 2012;161:505-522. https://doi.org/10.1016/j.jconrel.2012.01.043

89. Li M, Rouaud O, Poncelet D. Microencapsulation by solvent evaporation: state of the art for process engineering approaches. *Int J Pharm*. 2008;*363*:26-39. https://doi.org/10.1016/j.ijpharm.2008.07.018

90. Freytes DO, Martin J, Velankar SS, Lee AS, Badylak SF. Preparation and rheological characterization of a gel form of the porcine urinary bladder matrix. *Biomaterials*. 2008;*29*:1630-1637.

91. Williams BR, Gelman RA, Poppke DC, Piez K. Collagen fibril formation. Optimal in vitro conditions and preliminary kinetic results. *J Biol Chem*. 1978;*253*:6578-6585.

92. Gelman RA, Williams BR, Piez KA. Collagen fibril formation. Evidence for a multistep process. *J Biol Chem*. 1979;*254*:180-186.

93. Chen P, Cescon M, Bonaldo P. The role of collagens in peripheral nerve myelination and function. *Mol Neurobiol*. 2015;*52*:216-225.

94. Gao X, Wang Y, Chen J, Peng J. The role of peripheral nerve ECM components in the tissue engineering nerve construction. *Rev Neurosci*. 2013;*24*:443-453. https://doi.org/10.1515/revneuro-2013-0022

95. Koopmans G, Hasse B, Sinis N. Chapter 19 the role of collagen in peripheral nerve repair. *Int Rev Neurobiol*. 2009;*87*:363-379.

96. Chanut-Delalande H, Fichard A, Bernocco S, Garrone R, Hulmes DJS, Ruggiero F. Control of heterotypic fibril formation by collagen V is determined by chain stoichiometry. *J Biol Chem*. 2001;*276*:52-59.

97. Brightman AO, Rajwa BP, Sturgis JE, McCallister ME, Robinson JP, Voytik-Harbin SL. Time-lapse confocal reflection microscopy of collagen fibrillogenesis and extracellular matrix assembly in vitro. *Biopolymers*. 2000;*54*:222-234.

98. Rubiano A, Simmons CS. Mesoscale, cantilever-based indentation device for mechanical characterization of soft matter and biological tissue. *bioRxiv*. 2019;*3542*. https://doi.org/10.1101/758342

99. Rosso G, Guck J. Mechanical changes of peripheral nerve tissue microenvironment and their structural basis during development. *APL Bioeng*. 2019;*3*:6107. https://doi.org/10.1063/1.5108867

100. Leach JB, Brown XQ, Jacot JG, Dimilla PA, Wong JY. Neurite outgrowth and branching of PC12 cells on very soft substrates sharply decreases below a threshold of substrate rigidity. *J Neural Eng*. 2007;*4*:26-34.

101. Sundararaghavan HG, Monteiro GA, Firestein BL, Shreiber DI. Neurite growth in 3D collagen gels with gradients of mechanical properties. *Biotechnol Bioeng*. 2009;*102*:632-643.

102. Georges PC, Miller WJ, Meaney DF, Sawyer ES, Janmey PA. Matrices with compliance comparable to that of brain tissue select neuronal over glial growth in mixed cortical cultures. *Biophys J*. 2006;*90*:3012-3018.

103. Osama I, Gorenkova N, McKittrick CM, et al. In vitro studies on space-conforming self-assembling silk hydrogels as a mesenchymal stem cell-support matrix suitable for minimally invasive brain application. *Sci Rep*. 2018;*8*:1655. https://doi.org/10.1038/s41598-018-31905-5

104. Samadian H, Vaez A, Ehterami A, et al. Sciatic nerve regeneration by using collagen type I hydrogel containing naringin. *J Mater Sci Mater Med*. 2019;*30*:107. https://doi.org/10.1007/s10856-019-6309-8

105. Hsiao TW, Tresco PA, Hlady V. Astrocyte spreading and migration on aggrecan–laminin dot gradients. *Biointerphases*. 2018;*13*:401. https://doi.org/10.1116/1.5001675

106. Renault-Mihara F, Okada S, Shibata S, Nakamura M, Toyama Y, Okano H. Spinal cord injury: emerging beneficial role of reactive astrocytes' migration. *Int J Biochem Cell Biol*. 2008;*40*:1649-1653. https://doi.org/10.1016/j.biocel.2008.03.009

107. Fitch M, Silver J. CNS injury, glial scars, and inflammation: inhibitory extracellular matrices and regeneration failure. 2011;*4*:294-301.

108. Anderson MA, Burda JE, Ren Y, et al. Astrocyte scar formation AIDS central nervous system axon regeneration. *Nature*. 2016;*532*:195-200. https://doi.org/10.1038/nature17623

109. Bathina S, Das UN. Brain-derived neurotrophic factor and its clinical implications. *Arch Med Sci*. 2015;*11*:1164-1178.

110. Yano H, Torkin R, Martin LA, Chao MV, Teng KK. Proneurotrophin-3 is a neuronal apoptotic ligand: evidence for retrograde-directed cell killing. *J Neurosci*. 2009;*29*:790-802.

111. Ornitz DM, Itoh N. Protein family review: fibroblast growth factors. *Genome Biol*. 2001;*2*:1-5.

112. Wilgus T, Growth A. Factor–extracellular matrix interactions regulate wound repair. *Adv Wound Care*. 2012;*1*:249-254.

113. Belair DG, Le NN, Murphy WL. Design of growth factor sequestering biomaterials. *Chem Commun*. 2014;*50*:651-668.

114. Schultz GS, Wysocki A. Interactions between extracellular matrix and growth factors in wound healing. *Wound Repair Regen*. 2009;*17*:153-162.

115. Park JW, Hwang SR, Yoon I. Advanced growth factor delivery systems in wound management and skin regeneration. *Molecules*. 2017;*22*(8):1259. https://doi.org/10.3390/molecules22081259

116. Zhang S, Uludağ H. Nanoparticulate systems for growth factor delivery. *Pharm Res*. 2009;*26*:1561-1580. https://doi.org/10.1007/s11095-009-9897-z

SUPPORTING INFORMATION

Additional supporting information may be found in the online version of the article at the publisher's website.